Beneficiation of Acid Mine Drainage (AMD): A viable option for the synthesis of goethite, hematite, magnetite, and gypsum – Gearing towards a circular economy concept

Beneficiation of Acid Mine Drainage (AMD): A viable option for the synthesis of goethite, hematite, magnetite, and gypsum – Gearing towards a circular economy concept

V Akinwekomi[1], J. P Maree[2], V Masindi[3,4&,5], C Zvinowanda[6], M. S Osman[3], S. Foteinis[3], L. Mpenyana-Monyatsi[1], E Chatzisymeon[7]

[1]Department of Environmental, Water and Earth Sciences, Faculty of Science, Tshwane University of Technology, Private Bag X680, Pretoria, 0001, South Africa (bologov@tut.ac.za).
[2]ROC Water Technologies, P O Box 70075, Die Wilgers, 0041, Pretoria, South Africa
[3]Council for Scientific and Industrial Research (CSIR), Built Environment (BE), Hydraulic Infrastructure Engineering (HIE), P.O Box 395, Pretoria, 0001, South Africa, Tel: +2712 841 4107, Fax: +27128414847, VMasindi@csir.co.za, masindivhahangwele@gmail.com
[4]Department of Environmental Sciences, School of Agriculture and Environmental Sciences, University of South Africa (UNISA), P. O. Box 392, Florida, 1710, South Africa
[5]Magalies Water, Scientific Services, Research & Development Division, Erf 3475, Stoffberg street, Brits, 0250, tel: 0123816602
[6]University of Johannesburg, Applied Chemistry Department, Corner Beit and Nind Streets, Doornfontein Campus, Johannesburg, South Africa
[7]School of Engineering, Institute for Infrastructure and Environment, University of Edinburgh, Edinburgh EH9 16 3JL, United Kingdom

Abstract

Pollution of water resources by acid mine drainage (AMD) has been an issue of primary concern in recent decades, since it negatively affects the environment and its suitability to foster life. As such, efforts to recover, valorise and beneficiate minerals acquired from AMD treatment process have been ongoing, albeit with minimal success. With that in mind, this study unpacks novel ways of beneficiating AMD via the synthesis of valuable minerals with myriads of industrial applications. To this end, real AMD was used to synthesize goethite, hematite, magnetite, and gypsum (product minerals). Drinking water was also reclaimed as part of the treatment process, hence rendering this system a zero-liquid-discharge (ZLD) process. For the synthesis of goethite, hematite, and magnetite, Fe(III) and Fe(II) were recovered via sequential precipitation in batch reactors. Lime was added to treated water to synthesize high-grade gypsum. Furthermore, reverse osmosis (RO) was employed to reclaim drinking water as per South African drinking water standards (SANS 241) specifications. Product minerals were ascertained using advanced analytical techniques. Concisely, this study proved that AMD can be beneficiated into valuable minerals, which could be utilized in a number of industrial applications. The profits from selling the product minerals can potentially aid in offsetting the running costs of the treatment process, hence making this

[1] Corresponding Author: Vhahangwele Masindi: email: masindivhahangwele@gmail.com

process self-sustainable. This will also foster the concept of circular economy and waste beneficiating, thus curtailing the impacts of AMD to different spheres of the environment.

Keywords: Acid Mine Drainage (AMD); geothite; hematite; magnetite; gypsum; drinking water

1 Introduction

Acid mine drainage (AMD) is predominated by Fe^{2+}/Fe^{3+}, Al^{3+}, Mn^{2+}, and SO_4^{2-}, amongst traces of other elements. As such, major elements in AMD renders mine water a promising source of Fe-based minerals and sulphate. These elements can be recovered for other defined applications. Furthermore, clean water can also be reclaimed for a wide array of defined uses, including drinking water as specified in different water quality guidelines, specifications and standards (Masindi et al., 2014, Masindi et al., 2017, Masindi et al., 2019b). Goethite (FeO(OH)), hematite (Fe_2O_3), and magnetite (Fe_3O_4) are commercially valuable minerals which can be synthesized using Fe-rich salts or are formed naturally by geological processes (Akinwekomi et al., 2017, Duuring et al., 2018, Ali et al., 2016). These minerals are used in a number of fields (biomedicine, agriculture, and environment) such as chromatic science, ferro-fluid technology, information and energy storage, biomedicine, and controlled drug delivery, coal washing and as adsorbents. This is attributed to their high surface area, magnetic properties, cohesion ability, stability at varying temperature gradients and reusability (Chmielewská et al., 2017, Ponomar, 2018, de Almeida Silva et al., 2017). Their non-toxic conduct and biocompatible applications can also be enriched further by special surface coating with organic or inorganic molecules, including surfactants, drugs, proteins, starches, enzymes, antibodies, nucleotides, non-ionic detergents, and polyelectrolytes. Furthermore, selected Fe-rich nanoparticles can also be directed to an organ, tissue, or tumour using an external magnetic field for hyperthermic treatment of patients. With an increase in demand, apart from using ore deposits earth scientists and engineers tend to synthesize these minerals using commercially available salts; however, this put pressure on natural resources and is contradictory to the sustainable development concept. In that regard, the quest for alternative routes and options for harnessing and recovering Fe(III)/ Fe(II) has been ongoing. Research studies have explored the use of different waste materials and streams for Fe-species recovery and beneficiation (Akinwekomi et al., 2017, de Almeida Silva et al., 2017).

In a previous work of our group, Akinwekomi et al. (2017) suggested that Fe(II)/Fe(III) can be recovered from AMD and can be employed for the synthesis of magnetite at 2:1 Fe(III)/(II) ratios. This was attributed to the fact that AMD, from South African coal basins, is predominated by Fe, Al, Mn, and SO_4^{2-} amongst other trace elements (Masindi et al., 2018a). The levels of these chemical species also depend on the host rock, hence impacting the composition of the resultant AMD. As such, taking into account the geology of the Gauteng Province and the Mpumalanga Province in South Africa, the resultant AMD is predominated by Fe and SO_4^{2-} (Masindi et al., 2017). This suggests that the South African AMD can be a viable option for Fe-species recovery via fractional and sequential precipitation (Masindi et al., 2018c). This has been thoroughly investigated by Masindi et al. (2018c), where it was highlighted that Fe (III) may be recovered from oxidised AMD, originating from decanting shafts in abandoned mines and from holding dams from underground pumping, whereas Fe (II) can be acquired from non-oxidised AMD in active and dysfunctional shafts as well. This makes it feasible for fractional, selective, and sequential precipitation of chemical components at varying pH gradients.

As reported in literature, goethite and hematite is typically synthesize via thermo-treatment, by calcining the recovered material at temperatures ranging from 80 up to 700°C (Katsuki et al., 2018, Ponomar et al., 2018, Sakthivel et al., 2010, Supattarasakda et al., 2013). On the other hand, the technological routes to synthesize magnetite nanoparticles encompass ball milling, chemical precipitation, thermal decomposition, electrochemical method, sol–gel method, supercritical fluid method, hydrothermal method, chemical co-precipitation, sono-chemical decomposition method, flow injection method, and nano-reactors (Suppiah and Abd Hamid, 2016, Wei and Viadero Jr, 2007, Akinwekomi et al., 2017, Ali et al., 2016). Among these methodologies, chemical-based synthesis methods are mostly adopted due to low production cost and high yield (Ali et al., 2016). In light of the above, this study will adopt a facile magnetite synthesis method which entails chemical co-precipitation of Fe-species [Fe(III)/ Fe(II)] at 2:1 ratio, as proposed in literature (Aali et al., 2018, Ahmed et al., 2013). Alkaline agents are mainly used as a seeding material for metals to precipitate. Our group has previously synthesize magnetite using real AMD (Akinwekomi et al., 2017), however, the possibility of synthesizing goethite and hematite using real AMD originating from the South African coal basins remains largely unknown and this study works towards this end. Specifically, our group had successfully utilize sodium salts to synthesize magnetite at 2:1 [Fe(III)/ Fe(II)] ratio, with nitrogen purging being employed to prevent the oxidation of Fe(II)

(Akinwekomi et al., 2017). Herein, we build on these results in a quest to complete a value chain synthesis process that entails the use of Fe-species recovered from AMD and explore their overarching application. As such, this innovative study comprise the first comprehensive appraisal, in design and execution, to examine the recovery of Fe(III)/Fe(II) species from real South African AMD and explore their potential applications in the synthesis of goethite, hematite and magnetite. Subsequently, pre-treated water, which is rich in $NaSO_4$, was then used for gypsum synthesis. To achieve that, lime was added into the system to take out the sulphate. Finally, the product water which is rich in monovalent (Na) ions was further purified by Reverse Osmosis (RO). The secondary aim was to reclaim drinking water from the treatment process, thus, making this process self-sustainable.

2 Materials and methods

2.1 Sampling

Coal mine-derived raw AMD was collected from the Mpumalanga Province, South Africa. The samples were pre-filtered using Macherey-Nagel MN 615-Ø125 mm filter papers to remove debris and suspended solids. The filtrates were stored in the lab at 4°C until use for Fe-species recovery experiments. Na_2CO_3 and NaOH were sourced from Sigma-Aldrich and used as the feed reagents for the recovery of Fe-species from the filtered samples.

2.2 Minerals recovery

2.2.1 Recovery of Fe(III) sludge by selective precipitation

100 L of AMD was transferred into a reactor, adding 0.5 ml of a 10% sodium carbonate solution, in a drop-wise fashion, as to adjust the pH from 2 to 4.5. The mixture was equilibrated for 30 minutes, at 500 rpm using an overhead agitator. The mixture was then left to settle, in order to separate the sludge from the supernatant. The supernatant was further filtered using a whatman gravity filter in order to recover valuable minerals. The Fe(III) rich precipitates/sludge was then stored and the resultant filtrate was taken for ferrous (Fe(II)) sludge production, as will discussed below, while the water was kept for further treatment.

2.2.2 Recovery of Fe(II) sludge by selective precipitation

A similar procedure with the one described for the recovery of Fe (III) sludge was also followed for the recovery of Fe(II) sludge, using the pre-treated (filtrated) AMD.

Specifically, approximately 80 L of the pre-treated AMD was transferred into a reactor. Then, 2.5 ml of a 10% sodium hydroxide solution was added into an air-tight reactor, in drop-wise fashion, however, in this case to adjust the pH from 4.5 to ≥ 8.5. Similarly, the mixture was equilibrated for 30 minutes, at 500 rpm using an overhead agitator. To avoid oxidation in the reactor, nitrogen gas was regularly purged in order to remove possible air leakages and secondary reactions. The resultant products were then filtered via gravity as mentioned in section 2.2.1 to separate the supernatant from sludge. The Fe(II) rich precipitates/sludge was then stored until use in subsequent experiments, the resultant filtrate was taken for ferrous (Fe(II)) sludge production and treated water analysis.

2.3 Minerals synthesis

2.3.1 Synthesis of goethite

The Fe(III) rich slurry was transferred into a heat resistant glass cylinder. The cylinder was then heated at 80 °C for 45 minutes to allow the formation of a desired Fe-species. The slurry was then cooled to attain the synthesized paste, thereafter; the paste was dried at room temperature for 24 hrs.

2.3.2 Synthesis of hematite

Similarly, as in section 2.3.1, the Fe(III) rich slurry was transferred into a heat resistant glass cylinder. The cylinder was then heated, however, in this case at 700 °C, for 45 minutes, to allow formation of a desired Fe-species. The resultant mineral was left to cool at room temperature, for 0.5 hrs, and then, it was then taken for characterisation.

2.3.3 Synthesis of magnetite nanoparticles

The individual recovered sludge, (Fe(III) and Fe(II) acquired from steps defined in section 2.2.1 and 2.2.2), were further used for the synthesis of magnetite, as described in Akinwekomi et a1. (2017). The chemical-based synthesis method was adopted, due to its low production cost and high yield. Specifically, magnetite was synthesized by adding a base (Na(OH)) to the aqueous mixture of Fe(II) and Fe(III) recovered from AMD at 1:2 molar ratio, resulting in black colour precipitate/sludge. The chemical reaction of Fe_3O_4 precipitation is given in equations 1 and 2 below. The overall reactions are written as follows:

$$Fe^{2+} + 2Fe^{3+} + 8OH \rightarrow Fe_3O_4 + 4H_2O \quad (1)$$

Under oxygen-free environment, a complete precipitation of Fe_3O_4 is likely to take place between pH 9 and 14, maintaining a molar ratio of Fe(III):Fe(II) at 2:1 (Ali et al., 2016). Here we opted for pH 10 (Akinwekomi et al., 2017). Magnetite nanoparticles were synthesized through a ratio of 2:1 co-precipitation of Fe(III) and Fe(II) for 30 minutes. The temperature and pH were maintained at 100 °C and 10, respectively. The resultant precipitate was separated from the supernatant using the filtration technique described in section 2.1. To avoid the oxidation of Fe_3O_4 as denoted below:

$$Fe_3O_4 + 0.25O_2 + 4{:}5H_2O \rightarrow 3Fe(OH)^{3+} \quad (2)$$

Nitrogen gas was regularly purged into the reactor; this was done to eliminate possible air leakages and secondary reactions. Furthermore, bubbling nitrogen gas also aid in reducing the size of synthesized nanoparticles (Ali et al., 2016). A schematic presentation of a stepwise recovery of Fe-species from AMD, along with the routes followed for the synthesis of goethite, hematite, magnetite and gypsum are outlined in **Figure 1**.

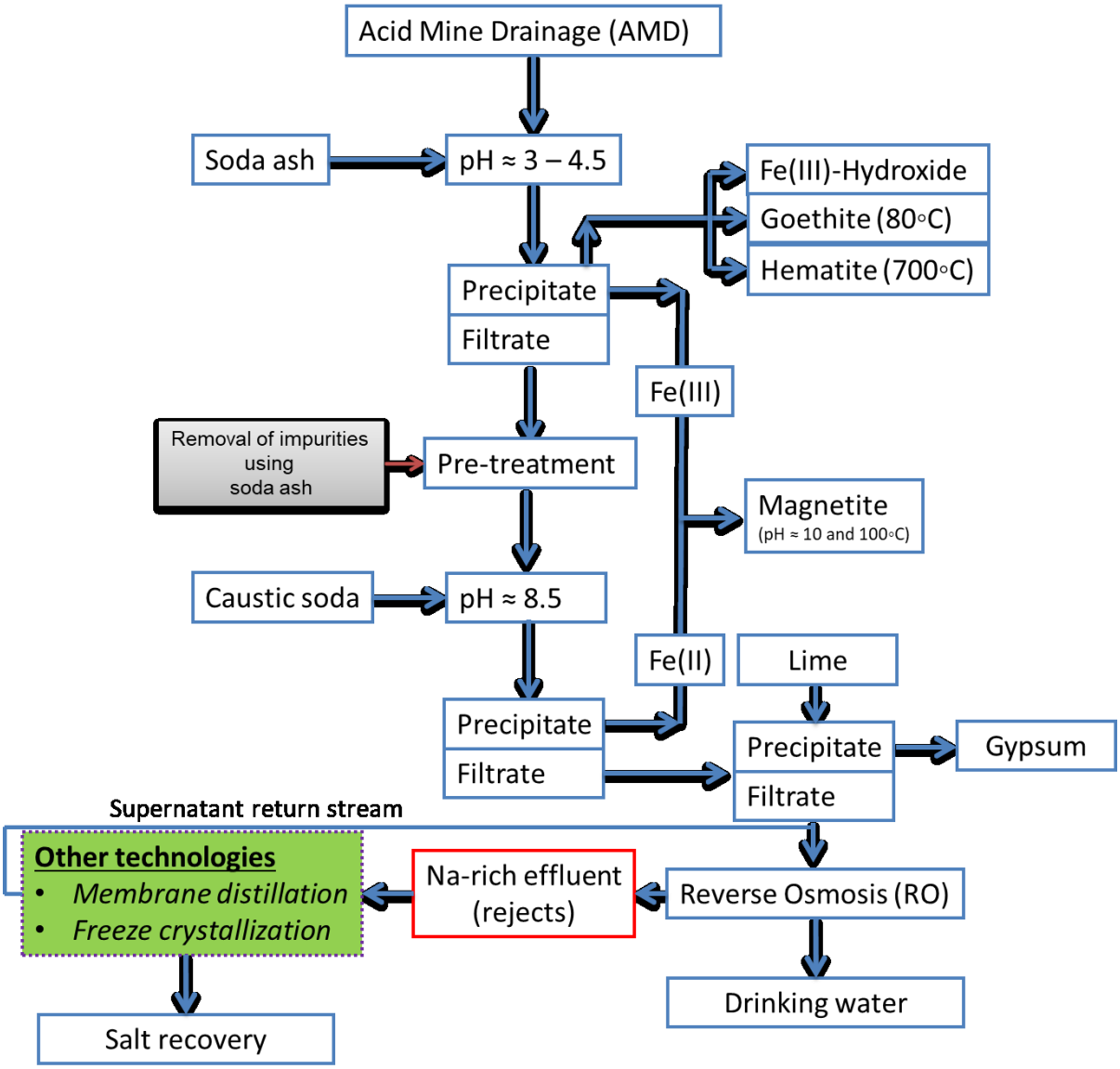

Figure 1: A schematic presentation of Fe-species recovery and routes followed for the synthesis of goethite, hematite, magnetite and gypsum. Figure adapted from Ryan et al. (2017).

2.3.4 Synthesis of gypsum

After the recovery of Fe-species, the treated water was rich in sulphate, which was recovered by adding 5 g of lime per L of treated water, thus leading to the formation of calcium sulphate (gypsum) (Liu et al., 2016). The product slurry was recovered as described in section 2.2.1 and then dried at 105 °C for 24 hrs. The dried gypsum sludge was milled into fine powder and packaged into Zip-Lock plastic bags until analysis, using the different analytical techniques described below.

2.3.5 Drinking water reclamation

The treated water, which was rich in mono-valent (Na ions) among other pollutants, was then transferred to a commercial RO facility for tertiary treatment. Specifically, a flat-sheet TFC-FO membrane from Porifera (Hayward, CA, USA) is used, able to operate at a wide pH range, from as low as 2 up to 13 pH (Table 1). It should be mentioned that both membrane layers are negatively charged for pH values higher than 4, and become more negative as pH is increases. Through this RO system high quality water was obtained, which was suitable for drinking according to the South African National Standard (SANS 241) in terms of inorganic contaminants.

2.4 Characterization

2.4.1 Feed Na-salts, recovered and synthesized dry solid samples

Determinations of the elemental and morphological properties of Fe-hydroxide, goethite, hematite, magnetite, and gypsum were carried out using High Resolution - Scanning Electron Microscope (HR- SEM) (Model: Sigma VP FE-SEM with Oxford EDS Sputtering System, Make: Carl Zeiss, Supplier: Carl Zeiss, USA) and High Resolution - Scanning Electron Microscope (HR- TEM) (JEM – 2100 electron microscope, Angus Crescent, Netherland). These pieces of equipment are coupled with an Energy Dispersive X-Ray Analysis/ Spectroscopy (referred to as EDX, EDAX, or EDS) system that enable the imaging capability of the microscope and the identified specimen of interest. EDS makes use of the X-ray spectrum, which is emitted by a solid sample when bombarded with a focused beam of electrons, as to obtain a localized chemical analysis. X-ray intensities are measured by counting the photons, while the obtained precision is limited by statistical error. The metal functional groups in Fe-hydroxide, goethite, hematite, magnetite, and gypsum were determined using Attenuated Total Reflection Fourier Transform Infrared Spectroscopy (ATR-FTIR). The infrared spectra were recorded at room temperature with a PerkinElmer Spectrum 100 Fourier Transform Infrared Spectrometer (FTIR), equipped with a PerkinElmer diamond Attenuated Total Reflectance (ATR) sampling accessory. The PerkinElmer Spectrum 100 FTIR is an optical system that gives data collection over the total range of 7800 to 370 cm^{-1}, with a best resolution of 0.5 cm^{-1} and consisting of a mid-infrared detector as standard (DTGS, deuterated triglycine sulphate). The instrument was connected to a PC which utilized Spectrum software to control the instrument and to record the spectra. The

powdered sample was placed on the crystal and a force was applied to ensure proper contact between the sample and the crystal. The spectral study was extended over the range 4000–400 cm^{-1}. Mineral compositions of Fe-hydroxide, goethite, hematite, magnetite and gypsum were acquired using powder X-ray diffraction patterns (XRD) obtained from a PANalytical X'Pert Pro powder diffractometer using Cu-Kα radiation with X'Celerator detector. XRD patterns taken at high angles ($2\theta \approx 10 - 90°$) were obtained using a step size of 0.02° and scan speed of 0.03° per second. The samples for the Na-based materials (feed minerals) and (synthesized & recovered) product minerals were prepared using a back loading preparation method. The phases were identified using X'Pert HighScore Plus software and the relative phase amounts (mass %) were estimated using the Rietveld quantitative analysis, a powerful method for determining the quantities of crystalline and amorphous components in multiphase mixtures (Philips PW 1710 Diffractometer; graphite secondary monochromatic source). These analyses were performed at the National Centre for Nanostructured Materials (NCNSM) of the Council for Scientific and Industrial Research (CSIR), Pretoria, South Africa.

2.4.2 Aqueous samples

HANNA, H98194 pH/EC/DO multi-parameter probe was used to monitor the pH, electrical conductivity (EC), total dissolved solids (TDS) and dissolved oxygen (DO) before and after Fe-species recovery. The levels of chemical species were determined using inductively coupled plasma-mass spectrometry (ICP-MS) (7500ce, Agilent, Alpharetta, GA, USA).

3 Results and discussions

3.1 Morphological properties of recovered and synthesized Fe-species

The morphological properties of Fe-hydroxide, goethite, hematite, magnetite, and gypsum, obtained by the HR- SEM, are shown in **Figure 2 (A – J)**.

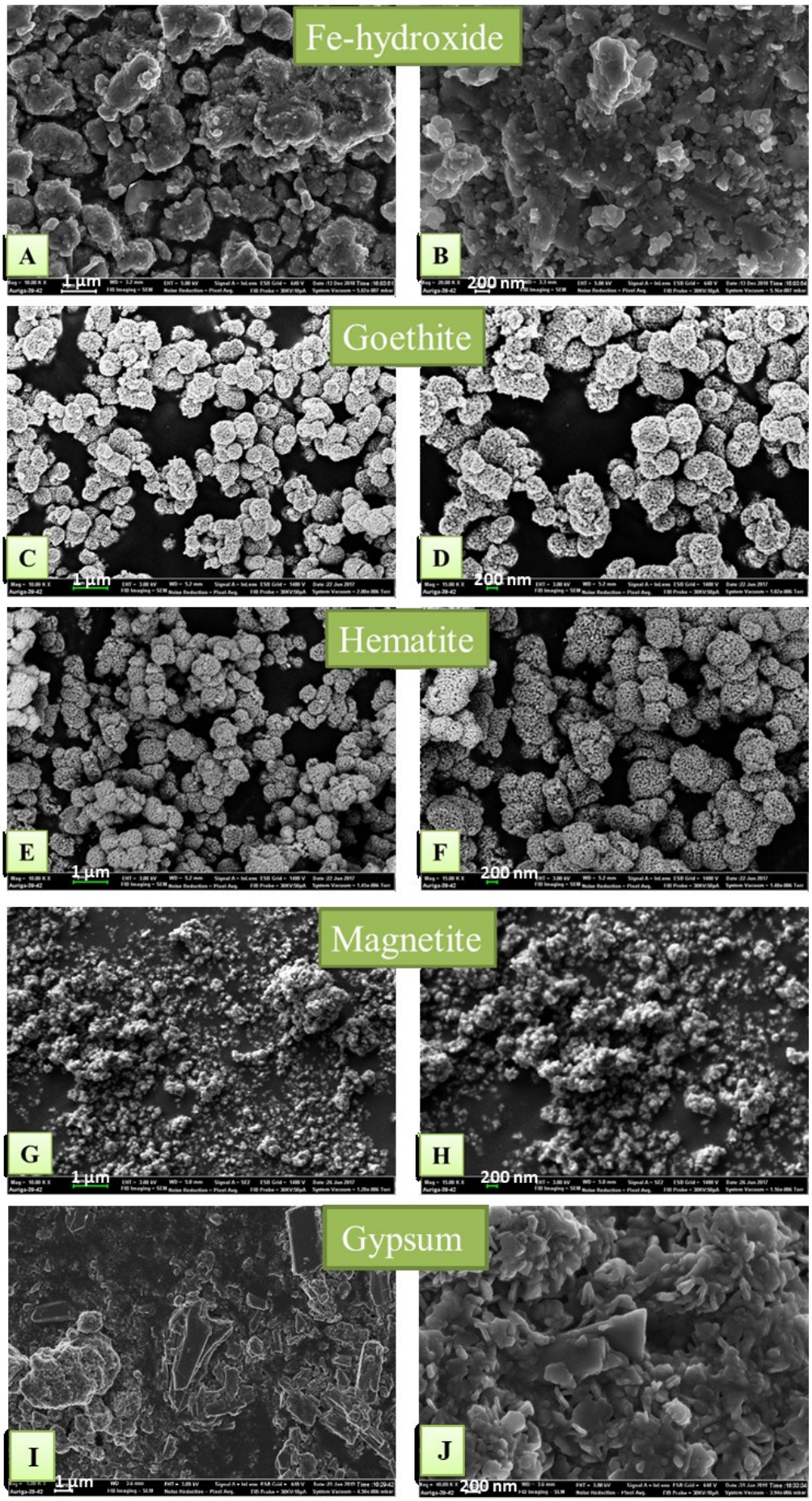
Fe-hydroxide
A
1 µm
B
200 nm
Goethite
C
1 µm
D
200 nm
Hematite
E
1 µm
F
200 nm
Magnetite
G
1 µm
H
200 nm
Gypsum
I
1 µm
J
200 nm

Figure 2: Morphological properties of Fe-hydroxide (A-B), goethite (C-D), hematite (E-F), magnetite (G-H), and gypsum (I-J).

Morphological properties are important in determining the homogeneity or heterogeneity of the material. This gives an indication on the uniformity of the material. As shown in **Figure 2 (A and B)**, the recovered Fe-hydroxide was observed to contain nanosheet-like structures of varying sizes compacted together. This indicates that the material is uniform. Furthermore, the goethite was observed to contain spherical structures with small spherical aggregates (**Figure 2 – C and D**). These were uniform, hence suggesting that the synthesized material is of high purity. In **Figure 2 (E and F)** it can be seen that hematite had spherical microstructures, with small spherical structures sandwiched together. This demonstrates that the synthesized material is uniform and very pure as well. As shown in **Figure 2 (G and H),** the magnetite nanoparticles were observed to contain spherical particles glued together. The particles were of similar size and they were also distributed across the surface of the analysed material. Finally, as shown in Figure 2 (I and J), gypsum contained rod-like structures lumped together in a uniform fashion. This indicates that the material is uniform and consists of similar minerals throughout its surface. Similar results have been reported in literature (Masindi et al., 2018b, Masindi et al., 2019a). As will discussed below the these results corroborate the results of the elemental mapping of the generated mineral phases, shown in Figure 3.

3.2 Elemental mapping of the recovered and synthesized Fe-species

Elemental mappings of Fe-hydroxide, goethite, hematite, magnetite, and gypsum were obtained using the HR-SEM-EDS Results are shown in **Figure 3 (A – E).**

Specifically, as shown in **Figure 3 (A – C),** granular like structures were observed on the surface of recovered material. This is a clear indication that calcination did not affected the morphology of the recovered Fe-species. Furthermore, **Figure 3D** shows that magnetite has boulder like morphology, with an even distribution of Fe and O, hence suggesting the presence of a Fe-O mineral, such as magnetite. Furthermore, **Figure 3E** shows the presence of rod-like structures, as was shown in the SEM images (Figure 2). These rods were uniform, hence indicating the dominances of minerals in their structure. The rods were also observed to contain Ca, O, and S as the main components in their matrices. This confirms a possible formation of gypsum. This was further ascertained by the FTIR and XRD results shown in section 3.3 and 3.4, respectively.

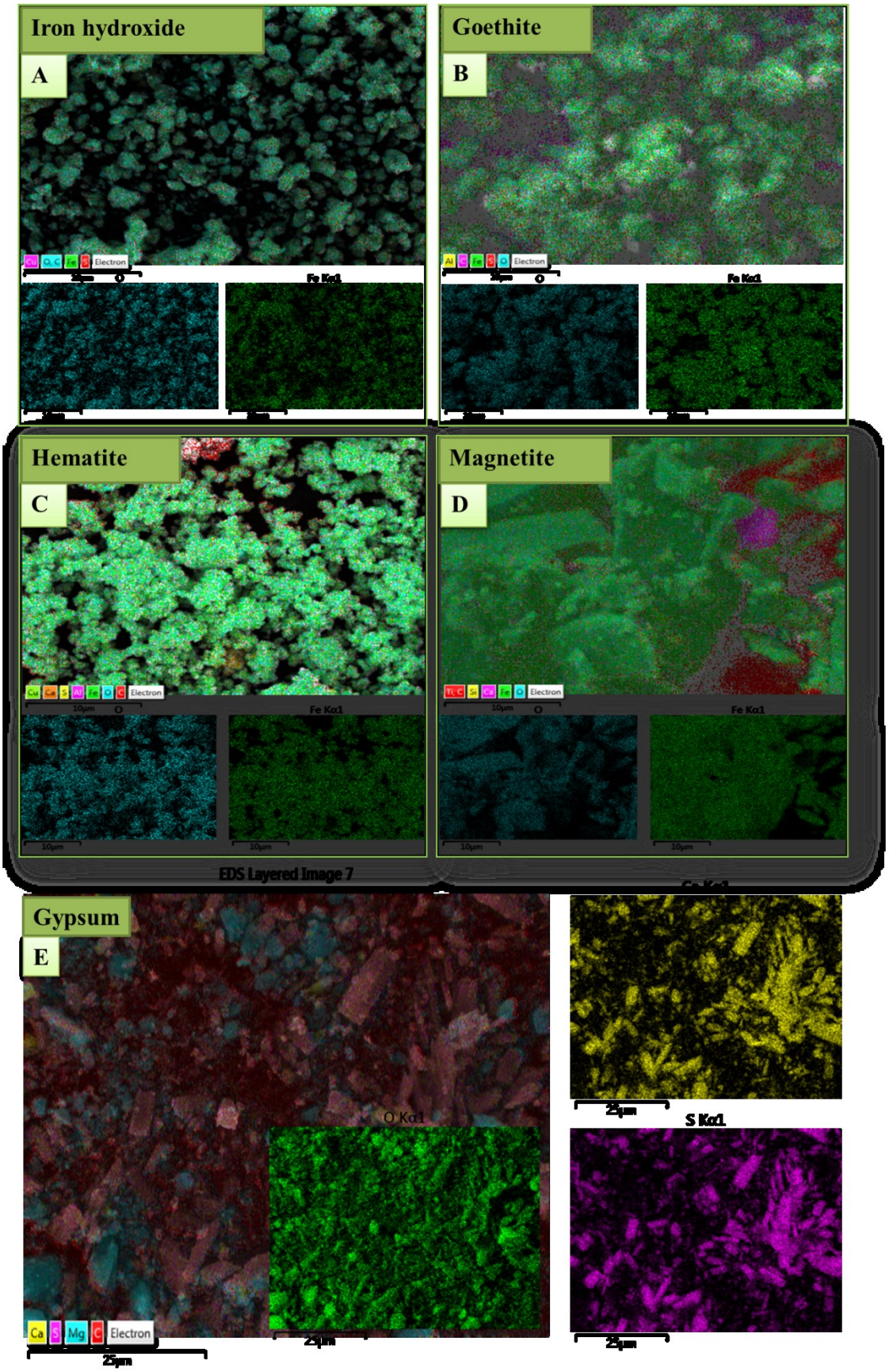

Figure 3: Elemental mapping of Fe-hydroxide, goethite, hematite, magnetite, and gypsum (A –E)

3.3 Morphological features obtained by HR-TEM

Results for the morphological properties of Fe-hydroxide, goethite, hematite, magnetite, and gypsum are shown in **Figure 4 (A – E)**.

Specifically, **Figure 4 (A and B)** depicts the morphology of Fe-hydroxide and goethite, which is observe to contain nano-tubes lumped together. However, according to **Figure 4C** hematite contains nanosheets, which are distributed across its surface. On the other hand, magnetite **(Figure 4D)** is observe to contain nano-rods distributed across its surface. **Figure 4E** shows the presence of rod-like structures within the matrices of the synthesized gypsum. The above corroborate the SEM-EDS results.

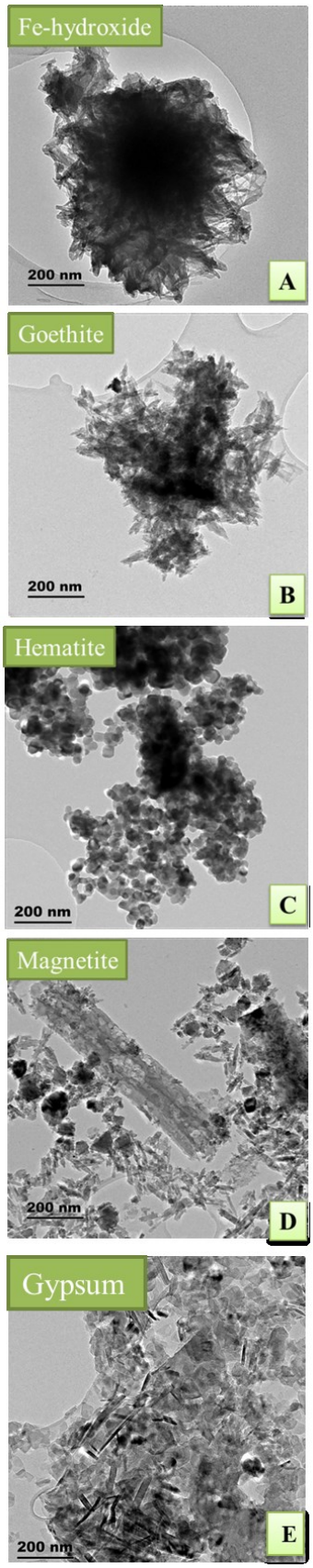

Figure 4: Morphological properties of Fe-hydroxide (A), goethite (B), hematite (C) and magnetite (E).

3.3 Metal functional groups for recovered and synthesized minerals

Results for metal functional groups for Fe-hydroxide, goethite, hematite, magnetite, and gypsum are shown in **Figure 5**.

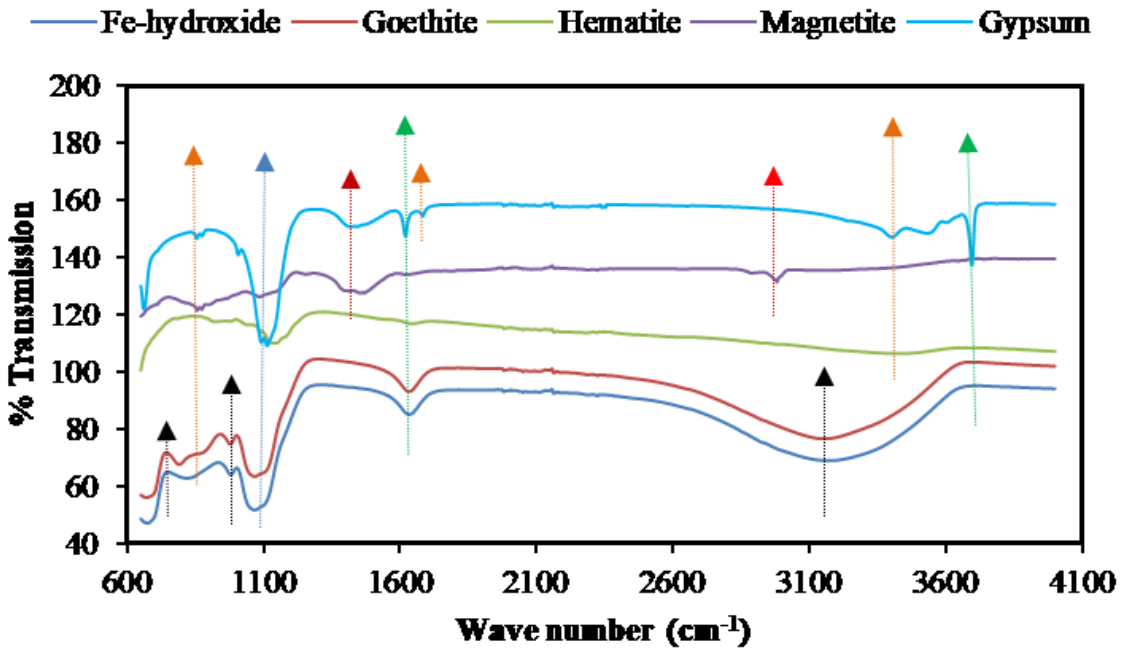

Figure 5: Metal functional groups of Fe-hydroxide, goethite, hematite, magnetite, and gypsum.

As shown in **Figure 5 and Table 1**, the recovered and synthesized Fe-hydroxide, goethite, hematite and magnetite were rich in Fe and OH groups, hence revealing that indeed these are Fe rich minerals. Furthermore, the presence of S-O group suggests the adsorption of sulphate species from AMD, since it is one of its main components. This further corroborates the XRD results. Furthermore, the presence of S-O and Ca duplex in the synthesized gypsum confirms that indeed gypsum is synthesized when lime is added. This is in-line with the SEM-EDS mapping and the XRD results.

Table 1: Metal functional groups for recovered and synthesized Fe-hydroxide, goethite, hematite and magnetite.

Mineral	Range (cm^{-1})	Metal functional	Reference
Fe-hydroxide	720	Fe-O	(Ramirez-Muñiz et al., 2018, Li et al., 2017, Guo et al., 2016, Jaiswal et al., 2013, Frost et al., 2005)
	850	Fe-O	
	1020	Fe-O-OH	
	1100	S-O or S=O	
	1660	H_2O molecule	
	3150	-OH group	
Goethite	720	Fe-O	(Ramirez-Muñiz et al., 2018, Li et al., 2017, Guo et al., 2016, Jaiswal et al., 2013, Frost et al., 2005)
	850	Fe-O	
	1020	Fe-O-OH	
	1100	S-O or S=O	
	1660	H_2O molecule	
	3150	-OH group	
Hematite	900	Fe-O	(Asoufi et al., 2018, Rufus et al., 2019, Kefeni et al., 2018)
	1100	S-O or S=O	
	3400	-OH group	
Magnetite	895	Fe-O	(Naeimi and Ansarian, 2018, Saxena and Singh, 2017, Azadi et al., 2018, Dash et al., 2019, Suppiah and Abd Hamid, 2016, Molina et al., 2019, Hadadian et al., 2018, Tahar et al., 2018, Shahid et al., 2018, Taimoory et al., 2018)
	1100	S-O or S=O	
	1400	Fe-O	
	1500	Fe-O	
	3000	-OH group	
Gypsum	1100	S-O or S=O	(Pouria et al., 2012, Shillito et al., 2009, Wang et al., 2017, Yan et al., 2014,
	1620 and 1680	H_2O duplex	
	3200 - 3700	-OH group	

			Zuhaimi et al., 2015)

3.4 Mineralogical properties analysis by X-ray diffraction (XRD)

The mineralogical compositions of the synthesized goethite, hematite, magnetite and gypsum are shown in **Figure 6**, while a discussion for each recovered mineral is shown below**.**

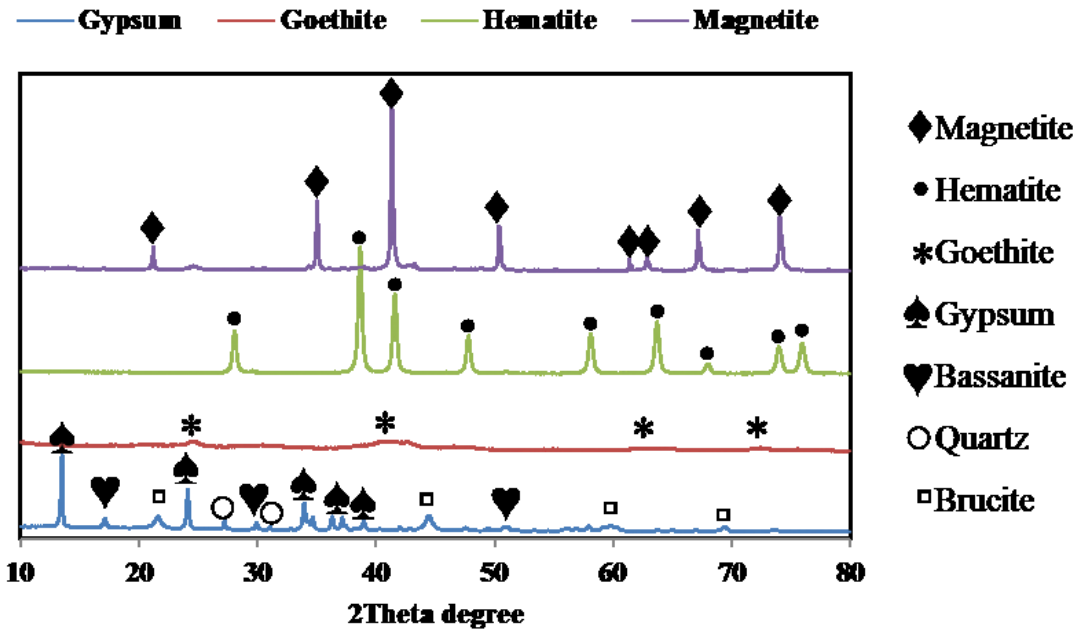

Figure 6: The mineralogical composition of the synthesized goethite, hematite, magnetite and gypsum. (Note: Goethite (FeO(OH)), hematite (Fe_2O_3), and magnetite (Fe_3O_4), Gypsum ($CaSO_4$. H_2O), Bassanite ($CaSO_4$. $12H_2O$), Quartz (SiO_2) and Brucite ($Mg(OH)_2$)).

3.4.1 Goethite

As shown in **Figure 6,** the presence of goethite is confirmed by the predominant peaks observed at 25, 39, 41, 43, 47, 63, and 74 theta degrees. A number of authors has reported similar results (Yang et al., 2017, Taleb et al., 2016, Ristić et al., 2013). Furthermore, the XRD pattern revealed that the synthesized product contained iron oxide nanoparticles both in crystalline and in amorphous state. Finally, the obtained quantitative results revealed that the synthesized goethite is 100% in purity, which suggests that could be a viable mineral for industrial applications. Lack of peaks Goethite denotes that the material is rich in amorphous fractions..

3.4.2 Hematite

The mineralogical composition and quantitative analysis of hematite synthesized from raw AMD was determined from the XRD pattern shown in **Figure 6**. Specifically, the XRD pattern revealed the orientation and crystalline nature of iron oxide nanoparticles. In addition, the characterisation results revealed that the synthesized hematite exhibited peaks at 27, 38, 40, 47, 58, 64, 69, 74, and 76 theta degrees. The observed peaks are in good agreement with the results reported by other researchers (Katsuki et al., 2018, Asoufi et al., 2018, Hu et al., 2018).

3.4.3 Magnetite

As illustrated in **Figure 6,** the XRD pattern revealed the good orientation and purely crystalline nature of iron oxide nanoparticles. Characterisation results for the synthesized magnetite revealed the presence of peaks at 21, 24, 35, 40, 50, 61, 63, 69, and 74 theta degrees. As such, the results obtained in this study are in agreement with the existing literature (Tipsawat et al., 2018, Bezdorozhev et al., 2017, Tahar et al., 2018). Moreover, quantitative results revealed that there was no presence of other peaks in magnetite's diffraction pattern, which, if existed, could suggest the existence of other impurities in the matrices of the synthesized mineral. Therefore, it is inferred that the synthesized magnetite is of high purity and good crystallinity, thus rendering this mineral viable for industrial applications.

3.4.4 Gypsum

Finally, as shown in **Figure 6,** the XRD pattern revealed the good orientation and purely crystalline nature of gypsum nanoparticles. Furthermore, the characterisation results for the synthesized gypsum revealed peaks at 20, 1, 5, 10, and 64 theta degrees, which suggests the presence of basanite, quartz, montomorillonite/smectite, brucite, and gypsum , respectively. The results of this study were consistent to the ones reported in literature (Magagane et al., 2019, Masindi et al., 2018c, Masindi et al., 2019a). Finally, the purity of the synthesized gypsum was observed to be 84%, which suggests its huge potential for a vast array of different applications in other defined uses. This further indicates that this material can be used as a source of gypsum in industries and other agricultural practices.

3.5 Water quality characterization

The inorganic chemical composition of raw AMD, Na-rich treated AMD, lime treated product water and RO treated product water are listed in **Table 2**.

Table 2. The chemical composition of raw AMD, Na-salt treated AMD, lime treated product water and RO treated water

Parameters	**Units**	**AMD**	**Fe-recovery final stream**	**Gypsum synthesis final stream**	**Reverse osmosis final stream**
Alkalinity (as $CaCO_3$)	mg/L	<5.0 ±0.01	20 ±0.05	20 ±0.01	20 ±0.02
pH units	-	2 ±0.01	11 ±0.09	11 ±0.05	9.5 ±0.01
Aluminium (Al)	mg/L	500 ±0.5	0.001 ±0.1	0.001 ±0.1	0.001 ±0.1
Iron (Fe)	mg/L	7000 ±0.01	≤0.01±0.05	≤0.01±0.05	≤0.01±0.05
Manganese (Mn)	mg/L	100 ±0.009	0.05 ±0.01	0.05 ±0.01	0.01 ±0.02
Sodium (Na)	mg/L	10 ±0.5	5000 ±0.01	4000 ±0.01	0.05 ±0.05
Calcium (Ca)	mg/L	450 ±0.05	50 ±1.5	100 ±0.05	0.08 ±0.09
Magnesium (Mg)	mg/L	400 ±0.05	50 ±0.01	0.5 ±0.05	0.05 ±0.03
Silicon (Si)	mg/L	30 ±0.01	25 ±0.05	5 ±0.04	0.05 ±0.01
Sulphate (SO_4)	mg/L	8000 ±0.05	7000 ±0.05	50 ±0.02	0.01 ±0.05

As shown in **Table 2,** AMD was dominated by Fe^{2+}/Fe^{3+}, Al^{3+}, Mn^{2+}, and SO_4^{2-}, amongst traces of other minerals/pollutants. This corroborates what has been reported in literature, regarding its high environmental contamination and toxicity potential if left untreated (Fernando et al., 2018, Nleya et al., 2016, Sahoo et al., 2013, Simate and Ndlovu, 2014). Moreover, the pH was observed to be <2, hence confirming that this effluent is highly acidic in nature. This was also confirmed by the low alkalinity. Furthermore, the presence of Fe and SO_4^{2-} confirms that the examined AMD was a good specimen for the synthesis of goethite, hematite, magnetite and gypsum. A confirmation for the synthesis of Fe-species and gypsum could be explained by a drastic drop in the concentration of Fe and SO_4^{2-} in feed water.

This was further confirmed by XRD results. Regarding the tertiary treatment of the lime treated water, it was observed that the levels of Na and other contaminants were significantly removed when using the RO system. Even though, the treatment of the Na-rich effluent was not the primary focus of this study, research is ongoing in our laboratory.Focus is given on Membrane distillation and cooling technologies, with the final goal to reclaim more water and also synthesize valuable salts. It should be mentioned that drinking water by itself is a value resource in South Africa, a water scarce country, while the recovered minerals could also potentially result in revenue that will offset the high RO costs and assist towards making this process self-sustainable and efficient.

5 Pilot set-up for AMD beneficiation

The state of art treatment plant within the CSIR premises in South Africa is shown in **Figure 7**

Figure 7: The treatment plant at within CSIR premises in South Africa

This multi-function and multi-purpose plant can treat 2000 LPD of AMD. In addition, it can recovery, synthesized, and reclaim quantifiable among of valuable minerals for secondary

use. It has by-pass and return streams to enable switching of streams and functionalities alternation.

6 Conclusions

Here it was shown that, real coal mine-derived AMD was successfully beneficiated into goethite, hematite, magnetite, and gypsum. It was also shown that it is possible to reclaim drinking water as a process co-product. Specifically, Fe-species were recovered via a selective and fractional precipitation process. It was observed that Fe(III) can be recovered at pH 3 – 4.5, whereas Fe(II) can be recovered at pH ≥ 8.5. The recovered Fe-species were successfully used for the synthesis of goethite at 80°C, hematite at 700°C and magnetite nanoparticles at 100°C. A very high purity (>99 %) was observed across the recovered Fe-species, which suggests their potential for industrial applications.

Furthermore, high purity magnetite nanoparticles were successfully synthesized via the co-precipitation method. The obtained results were corroborated by XRD, FTIR and ICP-MS analyses. Specifically, SEM and TEM determined that the morphology of Fe-hydroxide, goethite, hematite and magnetite were nano-sheets, spherical, spherical aggregates, and spherical nano-particles, respectively. Finally, after the recovery of the Fe-species the resultant AMD water was treat using lime to recover sulphate and gypsum, while the final effluent was further treated using Reverse Osmosis (RO) to reclaim drinking water.

Overall, the findings of this study demonstrated the potential of beneficiating environmental pollutants, such as AMD which was the case study herein, by converting them from waste to useful resources (e.g. for pigments, adsorbents for other pollutants and other useful compounds). As such, the findings of this work can be used towards promoting waste beneficiating and circular economy in the wastewater treatment sector and beyond. This will also ensure that RSA and other countries meet and respond to the sustainable development goals (SDG's), specifically, Envisioning 2030 as per Goal number 6, 9 and 12. This study focuses on that since waste from AMD treatment will be reduced and valuable minerals are recycled for beneficial use.

Acknowledgement

The authors wish to express their gratitude to the Council for Scientific and Industrial Research (CSIR), Magalies Water (MW), Rand Water, University of South Africa (UNISA),

Tshwane University of Technology (TUT), and the University of Johannesburg (UJ) for extending their resources in ensuring that the goals of this study were realised.

References

Aali, H., Mollazadeh, S. & Khaki, J. V. 2018. Single-phase magnetite with high saturation magnetization synthesized via modified solution combustion synthesis procedure. Ceramics International, 44**,** 20267-20274.

Ahmed, M. A., Ali, S. M., El-Dek, S. I. & Galal, A. 2013. Magnetite–hematite nanoparticles prepared by green methods for heavy metal ions removal from water. Materials Science and Engineering: B, 178**,** 744-751.

Akinwekomi, V., Maree, J. P., Zvinowanda, C. & Masindi, V. 2017. Synthesis of magnetite from iron-rich mine water using sodium carbonate. Journal of Environmental Chemical Engineering, 5**,** 2699-2707.

Ali, A., Zafar, H., Zia, M., Ul Haq, I., Phull, A. R., Ali, J. S. & Hussain, A. 2016. Synthesis, characterization, applications, and challenges of iron oxide nanoparticles. Nanotechnology, Science and Applications, 9**,** 49-67.

Asoufi, H. M., Al-Antary, T. M. & Awwad, A. M. 2018. Green route for synthesis hematite (α-Fe2O3) nanoparticles: Toxicity effect on the green peach aphid, Myzus persicae (Sulzer). Environmental Nanotechnology, Monitoring & Management, 9**,** 107-111.

Azadi, F., Karimi-Jashni, A. & Zerafat, M. M. 2018. Green synthesis and optimization of nano-magnetite using Persicaria bistorta root extract and its application for rosewater distillation wastewater treatment. Ecotoxicology and Environmental Safety, 165**,** 467-475.

Bezdorozhev, O., Kolodiazhnyi, T. & Vasylkiv, O. 2017. Precipitation synthesis and magnetic properties of self-assembled magnetite-chitosan nanostructures. Journal of Magnetism and Magnetic Materials, 428**,** 406-411.

Chmielewská, E., Tylus, W., Drábik, M., Majzlan, J., Kravčak, J., Williams, C., Čaplovičová, M. & Čaplovič, Ľ. 2017. Structure investigation of nano-FeO(OH) modified clinoptilolite tuff for antimony removal. Microporous and Mesoporous Materials, 248**,** 222-233.

Dash, A., Ahmed, M. T. & Selvaraj, R. 2019. Mesoporous magnetite nanoparticles synthesis using the Peltophorum pterocarpum pod extract, their antibacterial efficacy against pathogens and ability to remove a pollutant dye. Journal of Molecular Structure, 1178**,** 268-273.

De Almeida Silva, R., Menezes, J. C. S. D. S., Lopes, F. A., Kirchheim, A. P. & Schneider, I. a. H. 2017. Synthesis of a Goethite Pigment by Selective Precipitation of Iron from Acidic Coal Mine Drainage. Mine Water and the Environment**,** 1-7.

Duuring, P., Hagemann, S. G., Banks, D. A. & Schindler, C. 2018. A synvolcanic origin for magnetite-rich orebodies hosted by BIF in the Weld Range District, Western Australia. Ore Geology Reviews, 93**,** 211-254.

Fernando, W. a. M., Ilankoon, I. M. S. K., Syed, T. H. & Yellishetty, M. 2018. Challenges and opportunities in the removal of sulphate ions in contaminated mine water: A review. Minerals Engineering, 117**,** 74-90.

Frost, R., Yong Zhu, H., Wu, P. & Bostrom, T. 2005. Synthesis of acicular goethite with surfactants. Materials Letters, 59**,** 2238-2241.

Guo, X., Dong, H., Yang, C., Zhang, Q., Liao, C., Zha, F. & Gao, L. 2016. Application of goethite modified biochar for tylosin removal from aqueous solution. Colloids and Surfaces A: Physicochemical and Engineering Aspects, 502**,** 81-88.

Hadadian, Y., Sampaio, D. R. T., Ramos, A. P., Carneiro, A. a. O., Mozaffari, M., Cabrelli, L. C. & Pavan, T. Z. 2018. Synthesis and characterization of zinc substituted magnetite nanoparticles and their application to magneto-motive ultrasound imaging. Journal of Magnetism and Magnetic Materials, 465**,** 33-43.

Hu, X., Han, S. & Zhu, Y. 2018. Facet-controlled synthesis of polyhedral hematite/carbon composites with enhanced photoactivity. Applied Surface Science, 443**,** 227-235.

Jaiswal, A., Banerjee, S., Mani, R. & Chattopadhyaya, M. C. 2013. Synthesis, characterization and application of goethite mineral as an adsorbent. Journal of Environmental Chemical Engineering, 1**,** 281-289.

Katsuki, H., Choi, E.-K., Lee, W.-J., Hwang, K.-T., Cho, W.-S., Huang, W. & Komarneni, S. 2018. Ultrafast microwave-hydrothermal synthesis of hexagonal plates of hematite. Materials Chemistry and Physics, 205**,** 210-216.

Kefeni, K. K., Msagati, T. a. M., Nkambule, T. T. I. & Mamba, B. B. 2018. Synthesis and application of hematite nanoparticles for acid mine drainage treatment. Journal of Environmental Chemical Engineering, 6**,** 1865-1874.

Li, M., Liu, H., Chen, T., Hayat, T., Alharbi, N. S. & Chen, C. 2017. Adsorption of Europium on Al-substituted goethite. Journal of Molecular Liquids, 236**,** 445-451.

Liu, C., Zhao, Q., Wang, Y., Shi, P. & Jiang, M. 2016. Hydrothermal synthesis of calcium sulfate whisker from flue gas desulfurization gypsum. Chinese Journal of Chemical Engineering, 24**,** 1552-1560.

Magagane, N., Masindi, V., Ramakokovhu, M. M., Shongwe, M. B. & Muedi, K. L. 2019. Facile thermal activation of non-reactive cryptocrystalline magnesite and its application on the treatment of acid mine drainage. Journal of Environmental Management, 236**,** 499-509.

Masindi, V., Chatzisymeon, E., Kortidis, I. & Foteinis, S. 2018a. Assessing the sustainability of acid mine drainage (AMD) treatment in South Africa. Science of the Total Environment, 635**,** 793-802.

Masindi, V., Gitari, M. W., Tutu, H. & De Beer, M. 2014. Neutralization and attenuation of metal species in acid mine drainage and mine leachates using magnesite: a batch experimental approach. An Interdisciplinary Response to Mine Water Challenges**,** 640-644.

Masindi, V., Madzivire, G. & Tekere, M. 2018b. Reclamation of water and the synthesis of gypsum and limestone from acid mine drainage treatment process using a combination of pre-treated magnesite nanosheets, lime, and CO2 bubbling. Water Resources and Industry, 20**,** 1-14.

Masindi, V., Ndiritu, J. G. & Maree, J. P. 2018c. Fractional and step-wise recovery of chemical species from acid mine drainage using calcined cryptocrystalline magnesite nano-sheets: An experimental and geochemical modelling approach. Journal of Environmental Chemical Engineering, 6**,** 1634-1650.

Masindi, V., Osman, M. S. & Abu-Mahfouz, A. M. 2017. Integrated treatment of acid mine drainage using BOF slag, lime/soda ash and reverse osmosis (RO): Implication for the production of drinking water. Desalination, 424**,** 45-52.

Masindi, V., Osman, M. S. & Shingwenyana, R. 2019a. Valorization of acid mine drainage (AMD): A simplified approach to reclaim drinking water and synthesize valuable minerals - Pilot study. Journal of Environmental Chemical Engineering.

Masindi, V., Osman, M. S. & Shingwenyana, R. 2019b. Valorization of acid mine drainage (AMD): A simplified approach to reclaim drinking water and synthesize valuable minerals – Pilot study. Journal of Environmental Chemical Engineering, 7**,** 103082.

Molina, L., Gaete, J., Alfaro, I., Ide, V., Valenzuela, F., Parada, J. & Basualto, C. 2019. Synthesis and characterization of magnetite nanoparticles functionalized with organophosphorus compounds and its application as an adsorbent for La (III), Nd (III) and Pr (III) ions from aqueous solutions. Journal of Molecular Liquids, 275**,** 178-191.

Naeimi, H. & Ansarian, Z. 2018. Effective preparation of amine-functionalized nano magnetite as a precursor of novel solid acid catalyst for one-pot synthesis of

xanthenes under solvent-free conditions. Journal of the Taiwan Institute of Chemical Engineers, 85**,** 265-272.

Nleya, Y., Simate, G. S. & Ndlovu, S. 2016. Sustainability assessment of the recovery and utilisation of acid from acid mine drainage. Journal of Cleaner Production, 113**,** 17-27.

Ponomar, V. P. 2018. Thermomagnetic properties of the goethite transformation during high-temperature treatment. Minerals Engineering, 127**,** 143-152.

Ponomar, V. P., Dudchenko, N. O. & Brik, A. B. 2018. Synthesis of magnetite powder from the mixture consisting of siderite and hematite iron ores. Minerals Engineering, 122**,** 277-284.

Pouria, A., Bandegani, H., Pourbaghi-Masouleh, M., Hesaraki, S. & Alizadeh, M. 2012. Physicochemical properties and cellular responses of strontium-doped gypsum biomaterials. Bioinorganic Chemistry and Applications, 2012.

Ramirez-Muñiz, K., Perez-Rodriguez, F. & Rangel-Mendez, R. 2018. Adsorption of arsenic onto an environmental friendly goethite-polyacrylamide composite. Journal of Molecular Liquids, 264**,** 253-260.

Ristić, M., Opačak, I. & Musić, S. 2013. The synthesis and microstructure of goethite particles precipitated in highly alkaline media. Journal of Alloys and Compounds, 559**,** 49-56.

Rufus, A., Sreeju, N. & Philip, D. 2019. Size tunable biosynthesis and luminescence quenching of nanostructured hematite (α-Fe2O3) for catalytic degradation of organic pollutants. Journal of Physics and Chemistry of Solids, 124**,** 221-234.

Ryan, M. J., Kney, A. D. & Carley, T. L. 2017. A study of selective precipitation techniques used to recover refined iron oxide pigments for the production of paint from a synthetic acid mine drainage solution. Applied Geochemistry, 79**,** 27-35.

Sahoo, P. K., Kim, K., Equeenuddin, S. M. & Powell, M. A. 2013. Current approaches for mitigating acid mine drainage. Reviews of environmental contamination and toxicology, 226**,** 1-32.

Sakthivel, R., Vasumathi, N., Sahu, D. & Mishra, B. K. 2010. Synthesis of magnetite powder from iron ore tailings. Powder Technology, 201**,** 187-190.

Saxena, N. & Singh, M. 2017. Efficient synthesis of superparamagnetic magnetite nanoparticles under air for biomedical applications. Journal of Magnetism and Magnetic Materials, 429**,** 166-176.

Shahid, M. K., Phearom, S. & Choi, Y.-G. 2018. Synthesis of magnetite from raw mill scale and its application for arsenate adsorption from contaminated water. Chemosphere, 203**,** 90-95.

Shillito, L.-M., Almond, M. J., Nicholson, J., Pantos, M. & Matthews, W. 2009. Rapid characterisation of archaeological midden components using FT-IR spectroscopy, SEM–EDX and micro-XRD. Spectrochimica Acta Part A: Molecular and Biomolecular Spectroscopy, 73**,** 133-139.

Simate, G. S. & Ndlovu, S. 2014. Acid mine drainage: Challenges and opportunities. Journal of Environmental Chemical Engineering, 2**,** 1785-1803.

Supattarasakda, K., Petcharoen, K., Permpool, T., Sirivat, A. & Lerdwijitjarud, W. 2013. Control of hematite nanoparticle size and shape by the chemical precipitation method. Powder Technology, 249**,** 353-359.

Suppiah, D. D. & Abd Hamid, S. B. 2016. One step facile synthesis of ferromagnetic magnetite nanoparticles. Journal of Magnetism and Magnetic Materials, 414**,** 204-208.

Tahar, L. B., Oueslati, M. H. & Abualreish, M. J. A. 2018. Synthesis of magnetite derivatives nanoparticles and their application for the removal of chromium (VI) from aqueous solutions. Journal of Colloid and Interface Science, 512**,** 115-126.

Taimoory, S. M., Rahdar, A., Aliahmad, M., Sadeghfar, F., Hajinezhad, M. R., Jahantigh, M., Shahbazi, P. & Trant, J. F. 2018. The synthesis and characterization of a magnetite nanoparticle with potent antibacterial activity and low mammalian toxicity. Journal of Molecular Liquids, 265**,** 96-104.

Taleb, K., Markovski, J., Hristovski, K. D., Rajaković-Ognjanović, V. N., Onjia, A. & Marinković, A. 2016. Aminated glycidyl methacrylates as a support media for goethite nanoparticle enabled hybrid sorbents for arsenic removal: From copolymer synthesis to full-scale system modeling. Resource-Efficient Technologies, 2**,** 15-22.

Tipsawat, P., Wongpratat, U., Phumying, S., Chanlek, N., Chokprasombat, K. & Maensiri, S. 2018. Magnetite (Fe3O4) nanoparticles: Synthesis, characterization and electrochemical properties. Applied Surface Science, 446**,** 287-292.

Wang, S., Zhang, D., Ma, X., Zhang, G., Jia, Y. & Hatada, K. 2017. Spectroscopic and DFT study on the species and local structure of arsenate incorporated in gypsum lattice. Chemical Geology, 460**,** 46-53.

Wei, X. & Viadero Jr, R. C. 2007. Synthesis of magnetite nanoparticles with ferric iron recovered from acid mine drainage: Implications for environmental engineering. Colloids and Surfaces A: Physicochemical and Engineering Aspects, 294**,** 280-286.

Yan, Y., Dong, X., Sun, X., Sun, X., Li, J., Shen, J., Han, W., Liu, X. & Wang, L. 2014. Conversion of waste FGD gypsum into hydroxyapatite for removal of Pb2+ and Cd2+ from wastewater. Journal of Colloid and Interface Science, 429**,** 68-76.

Yang, X., Xia, L., Li, J., Dai, M., Yang, G. & Song, S. 2017. Adsorption of As(III) on porous hematite synthesized from goethite concentrate. Chemosphere, 169**,** 188-193.

Zuhaimi, N. a. S., Indran, V. P., Deraman, M. A., Mudrikah, N. F., Maniam, G. P., Taufiq-Yap, Y. H. & Ab. Rahim, M. H. 2015. Reusable gypsum based catalyst for synthesis of glycerol carbonate from glycerol and urea. Applied Catalysis A: General, 502**,** 312-319.